

A comprehensive study of Kepler phase curves and secondary eclipses – temperatures and albedos of confirmed Kepler giant planets

Daniel Angerhausen

Rensselaer Polytechnic Institute, 110 Eighth Street, Troy, NY 12180;
ORAU NASA Postdoctoral Fellow, NASA Goddard Space Flight Center, Greenbelt, MD
20771

Em DeLarme

Rensselaer Polytechnic Institute, 110 Eighth Street, Troy, NY 12180;
UCF, Planetary Sciences Group, Department of Physics, Orlando, FL 32816

and

Jon A. Morse

Rensselaer Polytechnic Institute, 110 Eighth Street, Troy, NY 12180;
BoldlyGo Institute, 1370 Broadway, 5th Floor Suite 572, New York, NY 10018

Received _____; accepted _____

submitted to PASP

ABSTRACT

We present a comprehensive study of phase curves and secondary eclipses in the Kepler data set using all data from 16 quarters that were available in 2013-2014. Our sample consists of 20 confirmed planets with $R_p > 4R_e$, $P < 10d$, $V_{mag} < 15$. Here we derive their temperatures and albedos, with an eye towards constraining models for the formation and evolution of such planets. Where there was overlap our results confirm parameters derived by previous studies, whereas we present new results for Kepler 1b-8b, 12b-15b, 17b, 40b, 41b, 43b, 44b, 76b, 77b, and 412b derived in a consistent manner. We also present lightcurve analyses for Kepler 91b and Kepler 74b, which both show extra dimmings at times other than from the expected primary and secondary eclipses. Corrected for thermal emission we find most of the massive planets from our sample to be low in albedo (< 0.1) with a few having higher albedo (> 0.1).

Subject headings: planets and satellites: atmospheres planets and satellites:
fundamental parameters planets and satellites: gaseous planets planets and satellites:
general

1. Introduction

1.1. The *Kepler* mission

Studying extrasolar planets is one of the major frontiers of astronomy today. The field has transformed from simple identification to comprehensive categorization and characterization of exoplanets and exoplanetary systems. Analyses of data provided by NASA’s *Kepler*¹ mission has revolutionized this field by compiling a statistically significant number of transiting planets and planetary candidates (e.g., Borucki et al. 2010b; Borucki et al. 2011; Batalha et al. 2013; Burke et al. 2014; Rowe et al. 2015; Mullally et al. 2015).

For example, *Kepler* data allowed researchers to discover Kepler 9b (Holman et al. 2010), the first multi-planetary system outside our solar system; Kepler 10b (Batalha et al. 2011), one of the first confirmed rocky planets outside the solar system; and Kepler 16b (Doyle et al. 2011), the first circumbinary planet. More recently the *Kepler* team announced the discovery of potentially habitable worlds in the Kepler 62 (Borucki et al. 2013) and Kepler 69 (Barclay et al. 2013) systems, and the near-Earth-sized planets Kepler-186f (Quintana et al. 2014) and Kepler-452b (Jenkins et al. 2015) in the habitable zones of their parent stars.

¹The data presented in this paper were obtained from the Mikulski Archive for Space Telescopes (MAST), which is managed by the Space Telescope Science Institute (STScI). STScI is operated by the Association of Universities for Research in Astronomy, Inc., under NASA contract NAS5-26555. Support for MAST for non-HST data is provided by the NASA Science Mission Directorate via grant NNX13AC07G and by other grants and contracts. This paper includes data collected by the *Kepler* mission. Funding for the *Kepler* mission is also provided by the NASA Science Mission Directorate.

Deeper analyses are possible using the exquisite *Kepler* data beyond merely detecting exoplanetary systems: researchers are now able to analyze large samples of planetary candidates to pin down occurrence rates such as η_{earth} (e.g., Howard et al. 2012; Dressing & Charbonneau 2013; Fressin et al. 2013; Petigura et al. 2013; Burke et al. 2015), find non-transiting planets via transit timing variations (Ballard et al. 2011), perform phase-curve analyses (Faigler et al. 2013), and may eventually even be able to detect exomoons (Kipping et al. 2013) and exotrojans (Hippke & Angerhausen 2015).

For the close-in, and therefore hot, planets around bright, high-signal host stars in the *Kepler* data set, we are able to analyze secondary eclipses, i.e., the modulated flux from the star-planet system when the light (reflection and thermal emission) of the planet disappears during its passage behind the parent star. Differential measurements then help us to characterize physical parameters of the planet such as albedo and temperature. Measuring such quantities, together with complementary spectroscopic measurements, can provide constraints on models for the formation and atmospheric photochemistry of such close-in planets (e.g., Line et al. 2010; Moses et al. 2011; Visscher & Moses 2011)

1.2. Transits and eclipses

Systems with transiting extrasolar planets can offer two important observational opportunities for deriving physical parameters of the planets. In *primary transit* the planet crosses the star. From a broadband transit-lightcurve, in this case, one can measure the planetary radius R_p in units of the stellar radius R_* . The depth of the transit is $\sim (R_p/R_*)^2$, which for a Jupiter radius planet transiting a sun-like star, is of the order of $\sim 1\%$ (e.g., Henry et al. 2000).

If the geometry (inclination, eccentricity) is right the planet also disappears behind its

Table 1. *Kepler* Quarters used in our analysis

KOI	LC Quarters	SC Quarters
1	0,1,2,3,4,5,6,7,9,10,11,13,14,15	0,1,2,3,4,5,6,7,8,9,10,11,12,13,14,15
2	0,1,2,3,4,5,6,7,8,9,10,11,12,13,14,15	0,1,2,3,4,5,6,7,8,9,10,11,12,13,14,15
3	0,1,2,3,4,5,6,8,9,10,12,13,14	0,1,2,3,4,5,6,8,9,10,11,12,13,14
7	0,1,2,3,4,5,6,7,9,10,11,13,15	0,1,2,3,4,5,6,7,9,10,11,13,14,15
10	0,1,2,3,4,5,6,7,8,9,10,11,12,13,14,15	1,2,3,4,5,6,7,8,9,10,11,12,13
13	0,1,2,3,4,5,6,7,8,9,10,11,12,13,14,15	1,2,3,6,7,8,9,10,11,12,13,14,15
17	0,1,2,3,4,5,6,8,9,10,12,13,14	1,2,3,4,5,6,8,9,10,11,12
18	0,1,2,3,4,5,6,7,8,9,10,11,12,13,14,15	1,2,3,4,5,6,7,8,9,10,11,12
20	0,1,2,3,4,5,6,7,9,10,11,13,14,15	1,2,3,4,5,6,7,8,9,10,11
97	0,1,2,3,4,5,6,7,8,9,10,11,12,13,14,15	2,3,4,5,6,7,8
98	0,1,2,3,4,5,6,7,8,9,10,11,12,13,14,15	2,3,4,5,6,7,8,9,10,11,12
127	1,2,3,4,5,6,7,8,9,10,11,12,13,14,15	2,3,4,5,6,7
128	1,2,3,4,5,6,7,8,9,10,11,12,13,14,15	2,3,4,5,6,7
135	1,2,3,4,5,6,7,8,9,10,11,12,13,14,15	2,3,4,5,6,7,9,10,11,12,13,14,15
196	1,2,3,4,5,6,7,8,9,10,11,12,13,14,15	3,4,5,6,7
200	1,2,3,4,5,6,7,8,9,10,11,12,13,14,15	3,4,5,6,7
202	1,2,3,4,5,6,7,8,9,10,11,12,13,14,15	3,4,5,6,7
203	1,2,3,4,5,6,8,9,10,12,13,14	3,4,5,6,7,8,9,10,11,12,13,14
204	1,2,3,4,5,6,7,8,9,10,11,12,13,14,15	3,4,5,6,7
428	1,2,3,4,5,6,8,9,10,12,13,14	–
1658	1,2,3,4,5,7,8,9,11,12,13,15	–
2133	0,1,2,3,4,5,6,7,8,9,10,11,12,13,14,15	–

Note. — For our analysis we used all data available prior to data release Q16, August 2013

host star in a so-called *secondary eclipse*. For a 2000 K hot Jupiter-size planet, the typical flux deficit during secondary eclipse is ~ 200 ppm at $\sim 2\mu\text{m}$ in the near-infrared and even larger at longer wavelengths, but considerably smaller at optical wavelengths (400-900 nm) at which *Kepler* observes. However, for host stars that are bright enough, *Kepler*'s outstanding sensitivity provides a direct measure of the planet's disk-averaged day side flux for some of its targets, particularly close-in gas giants – so called 'Hot Jupiters' and 'Hot Neptunes'.

Observing secondary eclipses combined with planetary phase curves can help us to characterize the planet and its atmosphere. For example, the depth of the secondary eclipse can constrain the albedo of the planet, while the timing and width of the secondary eclipse can help determine its orbital parameters. Comparing the amplitude of the reflected light in the phase curve with the depth of the secondary eclipse can constrain the day and night side temperatures, and therefore confirm the planetary nature of a candidate that is not self-luminous, and help to understand day to night side heat exchange. Measuring exoplanet eclipses, phase curves and albedo values yield information about the composition of their atmosphere, and day to night side temperature ratios yield the efficiency of energy transport and presence of possible temperature inversions (for details see, e.g., Cowan & Agol 2011).

Several previous studies have focused on eclipses and phase curves in the *Kepler* database, either on select samples of objects (e.g., Kipping & Bakos 2011 5 objects; Coughlin & López-Morales 2012 76 objects; Esteves et al. 2013 8 objects) or for individual planets or candidates (e.g., Mazeh et al. 2012; Morris et al. 2013).

In the largest sample so far, Coughlin & López-Morales 2012 modeled secondary eclipses and phase curves (only via a simple sinusoidal flux term applied to the lightcurves) of a uniform set of Hot Jupiter candidates from *Kepler* to derive albedos and thermal emission properties, and compared the results with stellar and planetary parameters. While

our study is similar in scope to this study, we worked with much more data (15 quarters – as available in August 2013 – of data instead of 1), a slightly bigger radius range (4 Earth radii = 0.4 Jupiter radii, instead of 0.5 Jupiter radii as a lower limit), and a longer period range (10 days instead of 5 days). Furthermore we applied a fully physical model with all different phase curve components. Of the Coughlin & López-Morales 2012 sample of 76 KOIs only 55 were successfully modeled with their methods. Of these 55 systems many still remain unconfirmed planetary candidates or turned out to be false positives (e.g., KOIs 102, 1419, 1459, 1541, 1543; <http://exoplanetarchive.ipac.caltech.edu/>, August 2015). For the confirmed planets there is significant overlap in our samples (KOIs 1, 2, 10, 13, 17, 18, 20, 97, 127, 128, 196, 202, 203, 204), but several planets in our study (KOIs 3, 7, 98, 135, 428 and 1658) were not covered by their analysis.

Here we present initial results of a comprehensive and consistent study of secondary eclipses and phase curves using data from quarters 0 through 15 of *Kepler* lightcurves (see Table 1), that were available at the time of our analysis. In this paper we focus on the 20 confirmed (August 2013) planets in the sample of 489 Kepler Objects of Interest (KOI) with $R_p > 4R_e$, $P < 10d$, and $V_{mag} < 15$. Consistent measurements of exoplanet phase curves not only allows us to break many current degeneracies in modeling the thermal and chemical structure of separate exoplanet atmospheres, but also enables us to compare results across the whole set of analyzed systems in a comprehensive way. Analyses like this will also help us prepare for future ground- and space-based facilities that increase the number of exoplanetary systems and the wavelength range of precision observations.

2. Data reduction

2.1. PyKE data preparation

For each of our targets, we used up to 16 quarters of the Pre-search Data Conditioning Simple Aperture Photometry (PDCSAP) lightcurves from the *Kepler* database available in the Mikulski Archive for Space Telescopes (MAST) at the time of our analysis (see Table 1; prior to the release of Q16 in Aug 2013)). The PDCSAP lightcurves are simple aperture photometry timeseries that have been cotrended in the *Kepler* pipeline to remove systematics common to multiple targets, using a best-fit of so-called ‘Cotrending Basis Vectors’ (CBVs). The CBVs are essentially the principal components of systematic artifacts for each science target and each operational quarter characterized by quantifying the features most common to hundreds of strategically-selected quiet targets sampled across the detector array (see Smith et al. 2012; Stumpe et al. 2012). Short-cadence data were used in place of long-cadence data when available and both data sets were combined weighted by their errors.

We used PyKE (Still & Barclay 2012), a series of python-based PyRAF recipes, for the individual and target-specific analysis and reduction of *Kepler* timeseries data. Our first step was to remove long-term variability using the `kepflatten` task to fit a quadratic polynomial to the baseline parts of the lightcurve for each quarter over time intervals of seven times the length of the published orbital period of each planet (see Table 2) using a sigma clipping of 2.5. We thus minimize any contamination or over-correction of the actual planetary phasecurves by the polynomial flattening and excluded the occultations. We then concatenated these flattened curves using the `kepstitch` routine, which created one long timeseries, containing all used quarters of data (see Table 1). Finally, using the `kepfold` task, we folded the entire lightcurve by the published orbital periods of each planet to get the phase curve, that was used in the next steps of our data analysis.

Table 2. System parameters used in phasecurve fits

KOI	reference	period [d]	T_{eff} [K]	$\log(g)$	$[Fe/H]$	u^a	y^a	R_p/R_* ^b	a/R_* ^b
1	Kepler Mission Team (2009)	2.47061317	5713	4.14	-0.14	0.62	0.38	0.124	8.445
2	Borucki et al. (2011)	2.20473537	6577	4.32	0.26	0.54	0.25	0.075	4.681
3	Bakos et al. (2010)	4.88780026	4780	4.59	0.31	0.72	0.55	0.057	16.68
7	Borucki et al. (2010a)	3.2136641	5857	4.25	0.17	0.61	0.36	0.025	6.47
10	Jenkins et al. (2010)	3.52249913	6213	4.28	-0.05	0.57	0.30	0.093	7.5
13	Kepler Mission Team (2009)	1.7635877	8848	3.93	-0.14	0.46	0.58	0.077	4.4
17	Dunham et al. (2010)	3.23469955	5647	4.23	0.34	0.64	0.40	0.093	7.53
18	Borucki et al. (2011)	3.54846566	5816	4.46	0.04	0.61	0.36	0.078	7.19
20	Fortney et al. (2011)	4.43796291	5947	4.17	0.07	0.60	0.34	0.117	8.133
97	Latham et al. (2010)	4.88548917	5933	3.98	0.11	0.60	0.34	0.082	6.842
98	Buchhave et al. (2011)	6.7901235	6395	4.11	0.12	0.55	0.29	0.056	7.299
127	Gandolfi et al. (2013)	3.57878272	5520	4.4	0.20	0.63	0.41	0.096	10.36
128	Kepler Mission Team (2009)	4.94278327	5718	4.18	0.36	0.64	0.39	0.101	10.34
135	Bonomo et al. (2012)	3.02409489	6041	4.26	0.33	0.59	0.33	0.0805	4.681
196	Santerne et al. (2011a)	1.85555773	5660	4.44	-0.09	0.62	0.39	0.096	5.99
202	Deleuil et al. (2014)	1.72086037	5750	4.3	0.27	0.61	0.38	0.099	5.22
203	Bonomo et al. (2012)	1.48571127	5781	4.53	0.26	0.61	0.37	0.129	5.67
204	Bonomo et al. (2012)	3.246732	5757	4.15	0.26	0.61	0.37	0.075	8.5
428	Santerne et al. (2011b)	6.8731791	6510	3.94	0.1	0.53	0.26	0.059	6.275
1658	Faigler et al. (2013)	1.54492977	6300	4.2	-0.1	0.53	0.28	0.085	4.61

^aimb- and gravity-darkening parameters derived from Claret & Bloemen (2011).

^bWhere needed parameters were given in units of stellar mass M_* and radius R_* and therefore independent of these values.

2.2. Phase curve model

We removed the primary transit signature as a first step in modeling the phase-folded lightcurves. The remaining normalized, out-of-transit phase curve F_{tot} was then modeled as

$$F_{tot} = f_0 + F_e + F_d + F_p + F_{ecl} \quad (1)$$

where F_{tot} is the sum of the stellar baseline f_0 (1 for normalized data) and the following four contributions to the lightcurve as a function of phase ϕ , with $\phi \in [0, 1]$, the primary transit at $\phi = 0$ and the secondary eclipse around $\phi = 0.5$ (for details on the various contributions see, e.g., Barclay et al. 2012, Shporer et al. 2010 or Groot 2012):

(i) F_e , the ellipsoidal variations resulting from tides on the star (of mass M_* and radius R_*) raised by the planet of mass M_p and semi-major axis a described by:

$$F_e = -A_e[\cos(2\pi 2\phi) + f_1 \cos(2\pi\phi) + f_2 \cos(2\pi 3\phi)] \quad (2)$$

where f_1 and f_2 are:

$$f_1 = 3\alpha(a/R_*)^{-1} \frac{5\sin^2(i) - 4}{\sin(i)} \quad (3)$$

$$f_2 = 5\alpha(M_p/M_*)(a/R_*)^{-3} \sin(i) \quad (4)$$

The parameter α is defined as

$$\alpha = \frac{25u}{24(15+u)} \frac{y+2}{y+1} \quad (5)$$

where u is the linear limb-darkening parameter and y is the gravity darkening parameter;

(ii) F_d , the Doppler boosting with amplitude A_d caused by the host star's changing radial velocity described by:

$$F_d = A_d \sin(2\pi\phi) \quad (6)$$

(iii) F_p , the planet’s phase function modeled as the variation in reflected light from a Lambertian sphere (Russell 1916) described by:

$$F_p = A_p \frac{\sin(z) + (\pi - z)\cos(z)}{\pi} \quad (7)$$

Here A_p is the amplitude of the planetary phase function, and z is related to phase ϕ and inclination i via:

$$\cos(z) = -\sin(i)\cos(2\pi\phi) \quad (8)$$

(iv) F_{ecl} , the secondary eclipse – i.e., the light that is blocked during the planet’s passage behind its host star – modeled using the description in Rogers et al. (2013), with $r(\phi)$, the separation between star and planet disk centers in the plane of the sky, in units of R_* , which we obtained from the referenced literature:

$$r(\phi) = (a/R_*)[1 - \sin^2(i)\cos^2(\phi - \phi_m)]^{1/2} \quad (9)$$

where ϕ_m is the phase of the mid-point of the secondary eclipse.

P_{ecl} is the eclipsed portion of the planet:

$$P_{ecl}(r) = \begin{cases} 0 & : r \geq 1 + p \\ f(\theta_1, \theta_2) & : 1 - p < r < 1 + p \\ 1 & : r \leq 1 - p \end{cases} \quad (10)$$

where p is $\frac{R_p}{R_*}$ and with

$$f(\theta_1, \theta_2) = \frac{1}{\pi p^2}(\theta_1 - \sin\theta_1 \cos\theta_1) \quad (11)$$

$$+ \frac{1}{\pi}(\theta_2 - \sin\theta_2 \cos\theta_2) \quad (12)$$

Here θ_1 and θ_2 are defined as:

$$\cos\theta_1 = \frac{1 + r^2 - p^2}{2r} \quad ; \quad \cos\theta_2 = \frac{r^2 + p^2 - 1}{2rp} \quad (13)$$

Hence the contribution F_{ecl} of the secondary eclipse with depth D_{ecl} is:

$$F_{ecl}(\phi) = D_{ecl}[1 - P_{ecl}(\phi, \phi_m)] \quad (14)$$

Here D_{ecl} is a positive value, with $F_{ecl} = D_{ecl}$ outside of secondary eclipse, such that the planet's light is visible for most of the orbit, and then $F_{ecl} = 0$ during secondary eclipse, as the planet's light is no longer visible.

2.3. Lightcurve fitting

We fit the cleaned (detrended and normalized with `kepflatten`) and phase-folded light-curves using MPFIT, an IDL package that implements Levenberg-Marquardt non-linear least squares curve fitting.

The errors on the parameters were obtained via the Levenberg-Marquardt fitting procedure, i.e., via the covariance matrix, which in some cases are likely to be underestimated

as this method does not take into account parameter correlations. The period was held constant because we were fitting phase-folded data. The limb and gravity darkening parameters were trilinearly interpolated from the tables of Claret & Bloemen (2011) and held constant during the fitting. The values for size ratio R_p/R_* and the distance between the planet and the star a/R_* as well as the used stellar parameters (e.g., $[Fe/H]$ or $\log(g)$) were obtained from the NASA Exoplanet Archive or the literature (see Table 2) and fixed in the fitting procedure. Given the short periods and tidal circularization timescales, we assumed a circular orbit for higher order effects (e.g., of e or ω) in the contributions of the various phase curve effects, so that they keep their analytic form. The contribution of these second-order effects is negligible and no error leakage occurred (with the exception of KOI-13, which has a significant eccentricity, see Figure 1 and Section 3.1.4). The depth of the secondary eclipse was constrained to be positive. Other parameters in the fit were the amplitude of the phase curve, the amplitude of the Doppler boosting, the amplitude of the ellipsoidal variations, the inclination, and the phase of the secondary eclipse. Restricting the depth of the secondary eclipse to be positive, along with the other fitted amplitudes, usually imparts a modeling bias towards higher positive values and more significant detections, especially if the signal is just above the noise level. Therefore we were very critical with marginal detections and tended towards null detections if the detected number was not significantly above the error level (see also discussion below and tables 3 and 5). For example in certain cases the fitted values for some of the phase contributions converged in the (non-zero) minimum value of 10^{-7} – in other words these contributions were not needed to fit the data. In these cases we inserted a conservative < 1 ppm in table 3.

In order to work on a uniform dataset and due to the computational intensity of fitting unbinned data, we cut out the transit part and binned all folded lightcurves down to 400 points for phase $\phi=[0.1,0.9]$ (the `kepfold` routine used in the previous step already ensured that short- and long-cadence data were combined properly in an error-weighted way).

While (Kipping 2010) showed that binning can induce morphological distortions to the photometric data light curve data of long cadence, we argue that the phase curve models work without a correction for this, as phase curve durations are significantly greater than the 30 minute cadence. For the secondary eclipse depths the integration time and binning will extend the secondary eclipse ingress and egress time, but those are very short compared to the eclipse duration.

We sought to include the best available parameters for the host stars in our modeling. Values from the Kepler Input Catalog (KIC) were often inaccurate, so we relied on the stellar parameters derived in the (mostly spectroscopic) planet confirmation observations (see Table2) available at the time of our analysis.

2.4. Temperatures and albedos

We calculated the brightness temperatures using:

$$D_{ecl} = (R_p/R_*)^2 \frac{\int B_\lambda(T_b)T_K d\lambda}{\int B_\lambda(T_*)T_K d\lambda} \quad (15)$$

where D_{ecl} is the depth of the secondary eclipse, R_p/R_* is the size ratio, B_λ is the Planck function, T_b is the brightness temperature, T_K is the *Kepler* response function, and T_* is the stellar temperature. To solve for T_b , we integrated the right-hand side of

$$\int B_\lambda(T_b)T_K d\lambda = D_{ecl}(R_*/R_p)^2 \int B_\lambda(T_*)T_K d\lambda \quad (16)$$

and then numerically integrated the left-hand side iteratively using successively larger temperature values, until we found the brightness temperature that best matched the measured depth of the secondary eclipse. The nightside temperatures are calculated in the same way, but using $F_{night} = F_{ecl} - A_p$ instead. If the difference between the phase curve and secondary eclipse was zero or negative, we did not calculate a night side temperature.

When the derived error bounds for some of the candidates included zero we did not give a lower limit for the night side temperature.

Furthermore, we calculated the geometric albedo using:

$$D_{ecl} = A_{g,obs}(R_p/a)^2 \quad (17)$$

which assumes no contribution from thermal emission.

Correcting for thermal emission we used (see Heng & Demory 2013):

$$A_{g,corr} = A_{g,obs} - \frac{\pi \int B_\lambda(T_{eq})d\lambda}{F_0}(a/R_*)^2 \quad (18)$$

where

$$F_0 = \sigma T_0^4 \quad (19)$$

with

$$T_0 = T_*(R_*/a)^{1/2} \quad (20)$$

Assuming a Lambertian criterion [$A_b = (3/2)A_g$] we calculated the equilibrium temperature using

$$T_{eq} = T_*(f_{dist}R_*/a)^{1/2}(1 - A_b)^{1/4} \quad (21)$$

The resulting albedos corrected for thermal emission for no redistribution, $f_{dist} = \frac{1}{2}$, and fully efficient redistribution, $f_{dist} = \frac{2}{3}$, of heat from planetary day to night side are shown in Table 5.

Cases where our derived night side temperatures resulted in upper limits indicate that the error in the night side flux was as large as the night side flux itself.

2.5. Phase shift due to clouds

For three of our targets (Kepler 7b, 12b and 43b) the fits using the phase curve model above were not sufficient and a clear systematic offset was seen in the residuals. A quick literature search for these targets from our sample showed that this effect can be explained by a shift of the reflection signal, due to the superrotation phenomenon (Demory et al. 2013; Heng & Demory 2013). In order to also model this higher order effect for these few exceptional systems, we added a component to the model lightcurve for (only) these three targets. This shift in the phase curve caused by planetary clouds (Demory et al. 2013) for Kepler 7b, 12b and 43b was modeled in a similar fashion to the phase curve itself, where we added an additional free parameter ϕ_{shift} to describe the phase shift:

$$\cos(z) = -\sin(i)\cos(2\pi(\phi + \phi_{shift})) \quad (22)$$

Using this model to modify F_p (updating equation 8 with equation 22) we found significant phase shifts ϕ_{shift} for KOI-20.01, KOI-97.01 and KOI-135.01 (see 3.1.7, 3.1.8, and 3.1.10).

2.6. Upper limits

For some of the planets in our sample we did not detect a secondary eclipse and/or a phase curve. In these cases we were only able to give upper limits for the derived parameters (see Section 3.2). In other cases our fits only constrained a limited number of parameters. For the planets in our sample for which the model does not fit a significant secondary eclipse, the upper limits for the secondary eclipse depths were calculated by adding the

1 sigma errors from the co-variance matrix to the best fit values. The same was applied and propagated for the then derived albedo and brightness temperature limits of these candidates (see Section 3.2).

3. Results

Our results are summarized in Tables 3 to 6. Figures 1 to 5 illustrate our fitting efforts. In the following subsections we report individually on all our analyzed targets and, where possible, compare to previous observations and measurements.

3.1. Detected secondary eclipses

3.1.1. KOI 1.01 / TrES-2b / Kepler 1b

TrES-2b (or KOI 1.01, Kepler-1b) – a $1.28 M_{Jup}$ and $1.24 R_{Jup}$ planet on a 2.47 day orbit around a G0V star (O’Donovan et al. 2006) – was the first planet detected in the *Kepler* field. Kipping & Spiegel (2011) determine a day night contrast amplitude of 6.5 ± 1.9 ppm which corresponds to a geometric albedo of $A_g = 0.025 \pm 0.007$ and found a non-significant eclipse with depth of 16 ± 13 ppm, similar to Kipping & Bakos (2011), who derived a value of 21 ± 22 . Demory & Seager (2011) found a geometric albedo of 0.06 ± 0.05 and an equilibrium temperature of 1464 K using only Q1 data. Barclay et al. (2012) derived a phase curve with ellipsoidal variations and Doppler beaming of amplitudes $2.79_{-0.62}^{+0.44}$ and $3.44_{-0.37}^{+0.32}$ ppm), respectively, and a difference between the day and night side planetary flux of $3.41_{-0.82}^{+0.55}$ ppm. They found a geometric albedo of $0.013_{-0.003}^{+0.002}$ and a secondary eclipse depth of $6.5_{-1.8}^{+1.7}$ ppm. Barclay et al. (2012) also showed that an atmosphere model that contains a temperature inversion is strongly preferred and suggested that the *Kepler* bandpass probes a significantly greater atmospheric depth on the night side. The analysis

of Esteves et al. (2013) for TrES-2b shows an eclipse depth of 7.5 ± 1.7 ppm, a brightness temperature T_b of 1910_{-50}^{+40} K a very low geometric albedo A_g of 0.03 ± 0.001 and a night side temperature T_{night} of 1700 K. For KOI-1.01 Coughlin & López-Morales 2012 ² measure an eclipse depth of -9.3 ± 14.2 ppm and report a maximum albedo of $-0.010_{-0.040}^{+0.04}$ and brightness temperature of -1700_{-243}^{+3563} K.

Our fit for KOI-1.01 shows an eclipse depth of 10.9 ± 2.3 ppm, a brightness temperature T_b of 1901_{-31}^{+27} a geometric albedo A_g of 0.05 ± 0.01 a bond albedo A_b of 0.08 ± 0.02 , leading to an upper limit for the night side temperature T_{night} of 1885_{-66}^{+51} K. These results agree very well with and therefore confirm the aforementioned measurements. Figure 1 (top, left) shows our fit results for KOI-1.01.

3.1.2. KOI 2.01 / HAT-P-7b / Kepler 2b

HAT-P-7b is a $1.78 M_{Jup}$ and $1.36 R_{Jup}$ planet on a 2.204 orbit around an evolved F6 star (Pál et al. 2008). Due to its bright host star and its detection before the launch of the *Kepler* mission it is one of the best studied planets in our sample. A number of other groups already analyzed the secondary eclipse of this target using different methods with results spanning from 67 up to 130 ppm. From the first 10 days of *Kepler* calibration data Borucki et al. (2009) derived an eclipse depth of 130 ± 11 ppm percent in the *Kepler* band. Using the whole first quartile Q1 data, Demory & Seager (2011) derived a geometric albedo of 0.20 ± 0.1 and an equilibrium temperature of 2085 K . Esteves et al. (2013) measure an eclipse depth of 68.31 ± 0.69 ppm, a brightness temperature T_b of 2846_{-4}^{+4} K a geometric

²When we cite values from Coughlin & López-Morales 2012 we use the results for their method 8 - "CLM Light Curve with Eccentricity Free and Stellar Parameters from from Isochrones" - from the supplement materials of their paper.

albedo A_g of 0.196 ± 0.002 and an upper limit for the night side temperature T_{night} of 1950 K for HAT-P-7. For KOI-2.01 Coughlin & López-Morales 2012 measure an eclipse depth of 57.7 ± 9.30 ppm and report a maximum albedo of $0.37^{+0.07}_{-0.060}$ and brightness temperature of $2860^{+65.00}_{-66}$ K.

For KOI-2.01, we find an eclipse depth of 69.3 ± 0.6 ppm, corresponding to a brightness temperature T_b of 2897^{+3}_{-4} K, a geometric albedo A_g of 0.27 ± 0.01 and a bond albedo A_b of 0.4 ± 0.01 . The resulting upper limit for the night side temperature T_{night} is 2235^{+3}_{-24} K. Here - again - we are mostly in agreement with the other analyses from the literature. Figure 1 (top, right) shows our fit results for KOI-2.01.

3.1.3. KOI 10.01 / Kepler 8b

Kepler 8b, with a radius of $1.41 R_{Jup}$ and a mass of $0.60 M_{Jup}$, is among the lowest density planets ($0.26 \frac{g}{cm^3}$) known. It orbits a relatively faint ($V = 13.89$ mag) F8IV subgiant host star with a period of $P = 3.523$ d and a semimajor axis of $0.0483^{+06}_{-0.0012}$ AU (Jenkins et al. 2010). Kipping & Bakos (2011) exclude secondary eclipses of depth 101.5 ppm or greater to $3\text{-}\sigma$ confidence, which excludes a geometric albedo > 0.63 to the same level. Demory & Seager (2011) report a geometric albedo of 0.21 ± 0.1 and an equilibrium temperature of 1567 K using only Q1 data. For Kepler 8b, Esteves et al. (2013) derive an eclipse depth of 26.2 ± 5.6 ppm, a brightness temperature T_b of 2370^{+50}_{-70} K a geometric albedo A_g of 0.134 ± 0.03 and an upper limit for the night side temperature T_{night} of 2100 K. For KOI-10.01 Coughlin & López-Morales 2012 measure an eclipse depth of -5.8 ± 45.9 ppm and report a maximum albedo of $0.36^{+0.36}_{-0.33}$ and brightness temperature of $2463^{+215.0}_{-587}$ K.

In our fits of KOI-10.01 we find an eclipse depth of 16.5 ± 4.45 ppm, a brightness temperature T_b of 2241^{+61}_{-77} K, a geometric albedo A_g of 0.11 ± 0.03 , a bond albedo A_b of

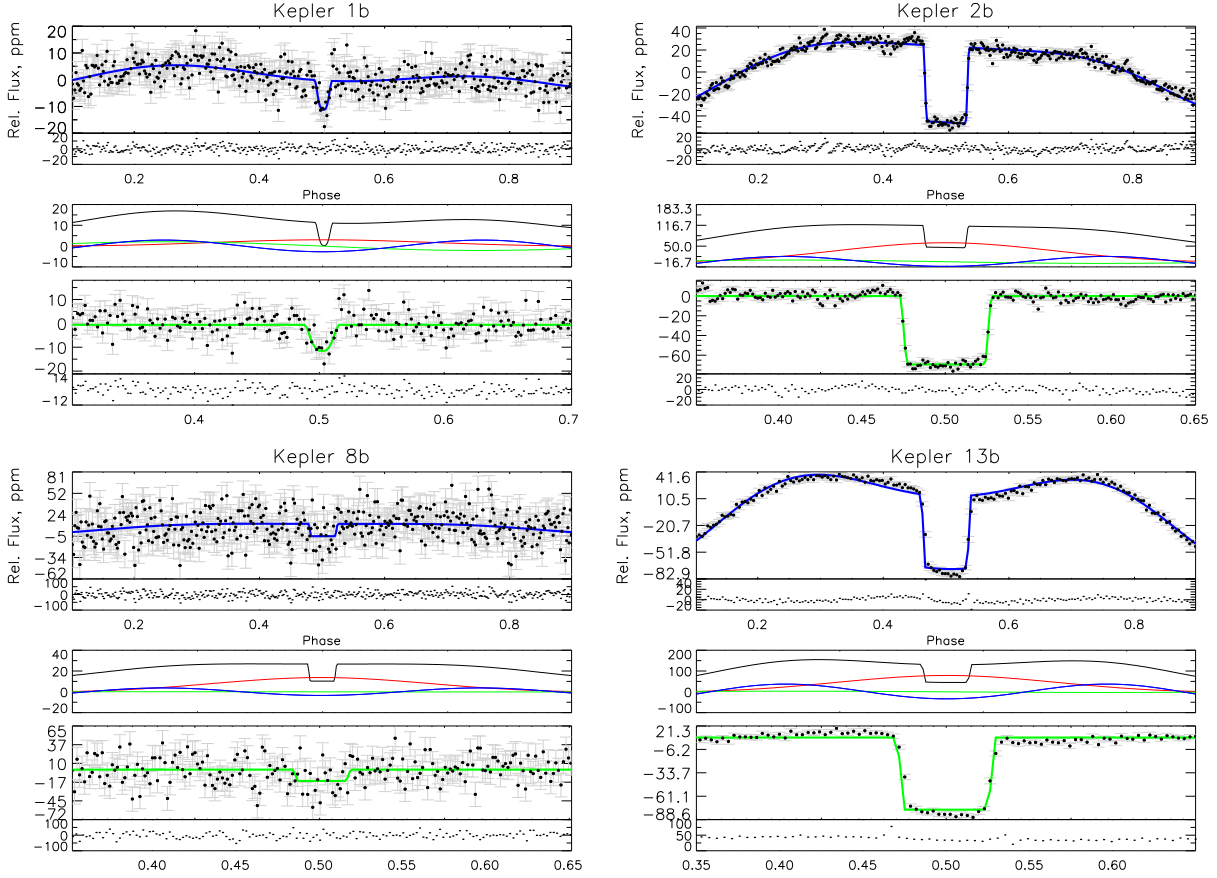


Fig. 1.— Fitted lightcurves for KOI-1.01/TrES-2b/Kepler 1b (top, left) KOI-2.01/HAT-P-7b/Kepler 2b (top, right), KOI-10.01/Kepler 8b (bottom, left) and KOI-13.01/Kepler 13b (bottom, right). In each quarter: Phase curve, residuals (top). Center: phase curve contributions: Doppler (blue), ellipsoidal (green), planetary phase (red). Bottom: zoom into phase curve subtracted secondary eclipse, residuals. Our model for KOI-13b shows a systematic offset from the actual data that may be explained by the system’s eccentricity (Placek et al. 2014) and/or gravity darkening (Masuda 2015).

0.16 ± 0.04 and an upper limit for the night side temperature T_{night} of 1859^{+227} K. Our results are slightly lower, however consistent with Esteves et al. 2013. Figure 1 (bottom, left) shows our fit results for Kepler 8b.

3.1.4. KOI 13.01 / Kepler 13b

Kepler 13 (or KOI 13.01) is the second brightest host star in our sample with mag 9.958 in the *Kepler* band. The planet Kepler 13b was detected by Shporer et al. (2011) due to its photometric orbit using the BEER algorithm (Faigler & Mazeh 2011). KOI-13.01 is a super-Jovian planet with a mass of $8.3 M_{Jup}$ and $1.4 R_{Jup}$ radius on a 1.76 day orbit around a A5-7V host star (Mislis & Hodgkin 2012). Santerne et al. (2012) found that the transiting planet is orbiting the main component of a hierarchical triple system of two fast rotating stars and one more companion with mass between 0.4 and $1 M_{Sun}$. Szabó et al. (2012) reported a spin-orbit resonance, transit duration variation and possible secular perturbations in the KOI-13 system. For KOI-13.01, Esteves et al. 2013 measure an eclipse depth of 143.0 ± 1.2 ppm, a brightness temperature T_b of 3706^{+5}_{-6} K a geometric albedo A_g of 0.42 ± 0.0031 and an upper limit for the night side temperature T_{night} of 2710. For KOI-13.01 Coughlin & López-Morales 2012 measure an eclipse depth of 88.8 ± 6.19 ppm and report a maximum albedo of $0.58^{+0.03}_{-0.030}$ and brightness temperature of $3758^{+55.00}_{-57}$ K.

For Kepler 13b, we find an eclipse depth of 84.8 ± 5.4 , corresponding to a brightness temperature of 3421^{+32}_{-35} , a geometric albedo of 0.27 ± 0.02 , a bond albedo of 0.40 ± 0.03 and a night side temperature of 2394^{+251} . Figure 1 (bottom, right) shows our fit results for Kepler 13b.

Part of the reason for the inconsistency with the Esteves et al. 2013 numbers is the different way the dilution between the two stars in the visual binary was accounted for also

the slightly different host star parameters assumed in each paper. Our results compare very well to the numbers of Shporer et al. 2014. However our fits show a clearly visual offset from the actual data (see 1; bottom, right – slope of the bottom of the secondary eclipse, excess flux prior to secondary). We suspect that the reported low but significant eccentricity of 0.034 ± 0.003 (Placek et al. 2014; Shporer et al. 2014) and gravity darkening (as shown in Masuda 2015) can explain this effect.

3.1.5. KOI 17.01 / Kepler 6b

Kepler 6b (Dunham et al. 2010) is a transiting Hot Jupiter orbiting a 3.8 Gyr old star with unusually high metallicity ($[\text{Fe}/\text{H}] = +0.34 \pm 0.04$) in a $P = 3.235$ d orbit. It has a mass of $M_P = 0.67 M_{Jup}$, and a radius of $R_P = 1.32 R_{Jup}$, resulting in a density of $0.35 (g/cm^3)$. The host star Kepler 6 is more massive and larger than the sun ($1.21 M_{Sun}$, $1.39 R_{Sun}$) but slightly cooler with $T_s=5724$ K. Kipping & Bakos (2011) exclude secondary eclipses of depth 51.5 ppm or greater to 3- σ confidence, which excludes a geometric albedo of more than 0.32 to the same level. Désert et al. (2011) found a brightness temperatures of Kepler 6b from Spitzer observations of $T_B = 1660 \pm 120$ K and an optical geometric albedo A_g in the *Kepler* bandpass of $A_g = 0.11 \pm 0.04$. Demory & Seager (2011) derive a geometric albedo of 0.18 ± 0.09 and an equilibrium temperature of 1411 K from *Kepler*'s Q1 data. For Kepler 6, Esteves et al. (2013) measure an eclipse depth of 8.9 ± 3.8 ppm, a brightness temperature T_b of 2000_{-100}^{+80} K, a geometric albedo A_g of 0.058 ± 0.025 and an upper limit for the night side temperature T_{night} of 1600 K. For KOI-17.01 Coughlin & López-Morales 2012 measure an eclipse depth of -71.7 ± 33.6 ppm and report a maximum albedo of $-0.33_{-0.27}^{+0.27}$ and brightness temperature of $-2306_{-163}^{+369.0}$ K.

For KOI-17.01, we derive an eclipse depth of 11.3 ± 4.2 ppm, a brightness temperature T_b of 2060_{-95}^{+70} K, a geometric albedo A_g of 0.07 ± 0.03 , a bond albedo A_b of 0.11 ± 0.04

and an upper limit for the night side temperature T_{night} of 1719^{+236} K - again confirming the results of Esteves et al. (2013). Figure 2 (top, left) shows our fit results for Kepler 6b.

3.1.6. KOI 18.01 / Kepler 5b

Kepler 5b (or KOI 18.01) is a $2.11 M_{Jup}$ and $1.43 R_{Jup}$ planet on a 3.55 day orbit around a 13th magnitude star (Koch et al. 2010). Kipping & Bakos (2011) detect a weak secondary eclipse for Kepler 5b of depth 25 ± 17 ppm and a geometric albedo of $A_g = 0.15 \pm 0.10$. Désert et al. (2011) found a brightness temperatures of Kepler 5b from Spitzer observations of $T_B = 1930 \pm 100$ K and an optical geometric albedo in the *Kepler* band of $A_g = 0.12 \pm 0.04$. Demory & Seager (2011) report a geometric albedo of 0.21 ± 0.1 and an equilibrium temperature of 1557 K using only Q1 data. For Kepler 5b, Esteves et al. (2013) find an eclipse depth of 18.8 ± 3.7 ppm, a brightness temperature T_b of 2400^{+50}_{-60} K, a geometric albedo A_g of 0.119 ± 0.025 and an upper limit for the night side temperature T_{night} of 2100. For KOI-18.01 Coughlin & López-Morales 2012 measure an eclipse depth of -89.8 ± 48.6 ppm and report a maximum albedo of $-0.47^{+0.51}_{-0.60}$ and brightness temperature of -2399^{+4274}_{-257} K.

Our lightcurve fits of KOI-18.01 show an eclipse depth of 19.8 ± 3.65 ppm, a brightness temperature T_b of 2305^{+46}_{-52} K, a geometric albedo A_g of 0.16 ± 0.03 , a bond albedo A_b of 0.25 ± 0.05 and a night side temperature T_{night} of 2169^{+81}_{-113} K. These results are very close to the values of Esteves et al. (2013). Figure 2 (top, right) shows our fit results for KOI-18.01.

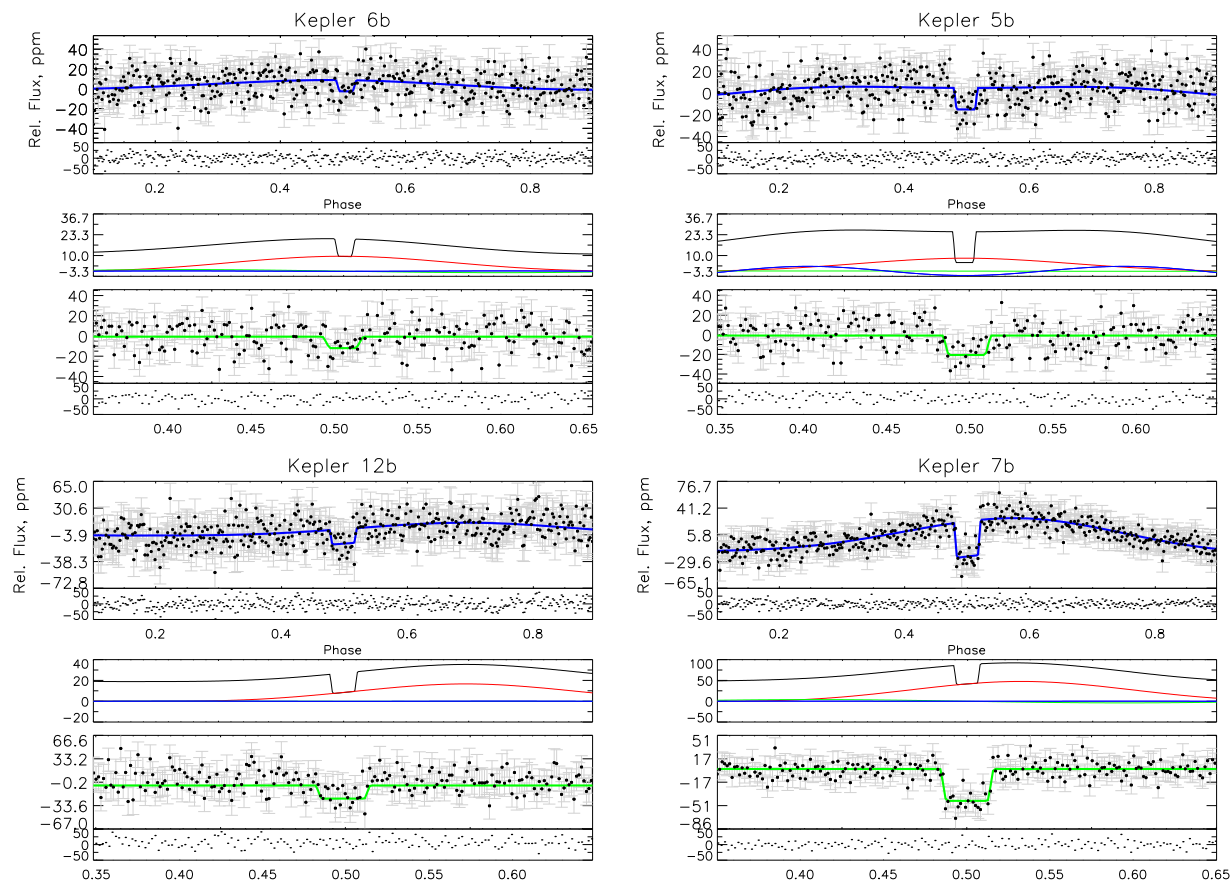


Fig. 2.— Fitted lightcurves for KOI-17.01/Kepler 6b (top, left) KOI-18.01/Kepler 5b (top, right), KOI-20.01/Kepler 12b (bottom, left) and KOI-97.01/Kepler 7b (bottom, right). In each quarter: Phase curve, residuals (top). Center: phasecurve contributions: Doppler (blue), ellipsoidal (green), planetary phase (red). Bottom: zoom into phase curve subtracted secondary eclipse, residuals.

3.1.7. KOI 20.01 / Kepler 12b

Kepler 12b (KOI 20.01, Fortney et al. 2011), with a radius of $1.69 \pm 0.03 R_{Jup}$ and a mass of $0.43 \pm 0.04 M_{Jup}$, belongs to the group of planets with highly inflated radii. On a 4.44 day orbit around a slightly evolved G0 host, Kepler 12b is the least irradiated within the class of inflated and very low density planets ($0.11 \pm 0.01 (g/cm^3)$) and may have important implications for the question of the correlation between irradiation and inflation. Fortney et al. (2011) also detected a secondary eclipse depth of 31 ± 7 ppm, corresponding to a geometric albedo of 0.14 ± 0.04 . For KOI-20.01 Coughlin & López-Morales 2012 measure an eclipse depth of -26.3 ± 28.5 ppm and report a maximum albedo of $0.16_{-0.13}^{+0.17}$ and brightness temperature of $2115_{-312}^{+180.0}$ K.

Our fits of KOI 20.01’s lightcurve confirm and improve this with a resulting eclipse depth of 18.7 ± 4.9 ppm, a brightness temperature T_b of 2121_{-67}^{+54} K, a geometric albedo A_g of 0.09 ± 0.02 , a bond albedo A_b of 0.14 ± 0.04 and an upper limit for the night side temperature T_{night} of 1711^{+223} K. Furthermore we found a phase shifts ϕ_{shift} of -0.19 ± 0.03 for KOI 20.01. Figure 2 (bottom, left) shows our fit results for Kepler 12b.

3.1.8. KOI 97.01 / Kepler 7b

Kepler 7b (Latham et al. 2010) with a mass of $0.43 M_{Jup}$ and radius $1.48 R_{Jup}$ also has a very low density of $0.17(g/cm^3)$. For KOI-97.01 Coughlin & López-Morales 2012 measure an eclipse depth of 79.1 ± 15.3 ppm and report a maximum albedo of $1.26_{-0.33}^{+0.36}$ and brightness temperature of $2626_{-101}^{+90.00}$. Demory et al. (2011), using Q0-Q4 data, measure an occultation depth in the *Kepler* bandpass of 44 ± 5 ppm, a geometric albedo of 0.32 ± 0.03 , and a planetary orbital phase light curve with an amplitude of 42 ± 4 ppm.

Our results for KOI-97.01 confirm this almost exactly: we find an eclipse depth of 46.6

± 4.0 ppm, a brightness temperature T_b of 2547_{-28}^{+26} K, a geometric albedo A_g of 0.32 ± 0.03 and a bond albedo A_b of 0.48 ± 0.04 . We also detected an additionally phase shifts ϕ_{shift} of -0.08 ± 0.02 for KOI-97.01. Figure 2 (bottom, left) shows our fit results for Kepler 12b. It is interesting to see that the error values for Demory et al. (2011) are almost exactly the same, even though they only used Q0-4 in comparison to Q0-15 in our study. One possible explanation could be that Demory et al. (2011) did not include Doppler or ellipsoidal components in their model or maybe these result hint at a systematic noise floor we are reaching here.

We also confirm the following results: Kipping & Bakos (2011) detect a secondary eclipse for Kepler 7b of depth 47 ± 14 ppm and a geometric albedo of $A_g = 0.38 \pm 0.12$. The day-night difference of 17 ± 9 ppm they calculate supports the hypothesis of thermal emission as a source for both the secondary eclipse and the phase curve. Demory & Seager (2011) find a geometric albedo of 0.35 ± 0.11 and an equilibrium temperature of 1370 K using only data from the first quartile.

3.1.9. KOI 127.01 / Kepler 77b

Kepler 77b (Gandolfi et al. 2013) is a moderately bloated planet with a mass of $M_P = 0.430 \pm 0.032 M_{Jup}$, a radius of $R_P = 0.960 \pm 0.016 R_{Jup}$, orbiting) G5 V star with a period of 3.58 days. Gandolfi et al. (2013) do not find a secondary eclipse with a depth larger than 10 ppm which leads to limits of the geometric and Bond albedo of $A_g \leq 0.087 \pm 0.008$ and $A_b \leq 0.058 \pm 0.006$, respectively. For KOI-127.01 Coughlin & López-Morales 2012 measure an eclipse depth of -92.6 ± 39.1 ppm and report a maximum albedo of $-1.11_{-0.41}^{+0.36}$ and brightness temperature of $-2563_{-112}^{+129.0}$ K.

For KOI-127.01, we find an eclipse depth of 13.3 ± 7.4 ppm, which results in a

brightness temperature of 2062_{-165}^{+100} K, geometric albedo of 0.15 ± 0.09 , bond albedo of 0.23 ± 0.13 and night side temperature of 1854^{+216} K. Figure 3 (top, left) shows our fit results for Kepler 77b.

3.1.10. KOI 135.01 / Kepler 43b

KOI-135.01 (Bonomo et al. 2012) with radius $R_P = 1.20 \pm 0.06 R_{Jup}$ and mass $M_P = 3.23 \pm 0.19 M_{Jup}$ orbits its parent star in 3.02 days. We are the first to report a secondary eclipse of KOI-135.01 with a depth of 17.0 ± 5.3 ppm. This corresponds to a brightness temperature T_b of 2296_{-95}^{+73} K, a very low geometric albedo A_g of 0.06 ± 0.02 and a bond albedo A_b of 0.09 ± 0.03 respectively. Using our model we also found a phase shift ϕ_{shift} of -0.10 ± 0.01 for KOI-135.01. Figure 3 (top, right) shows our fit results for KOI-135.01.

3.1.11. KOI 196.01 / Kepler 41b

The planet KOI-196.01, with a radius of $0.84 \pm 0.03 R_{Jup}$ and a mass of $0.49 \pm 0.09 M_{Jup}$, orbits a G2V star of $0.99 \pm 0.03 R_{sun}$ (Santerne et al. 2011a): KOI-196.01 is one the rare close-in Hot Jupiters with a radius smaller than Jupiter suggesting a non-inflated planet. Santerne et al. (2011a) detect a secondary eclipse depth of 64 ± 10 ppm as well as the optical phase variation, leading to a relatively high geometric albedo of $A_g = 0.3 \pm 0.08$ and a temperature of $T_B = 193 \pm 80$ K. Quintana et al. (2013) confirmed the Hot Jupiter Kepler 41b via phase curve analysis and find a secondary eclipse depth of 60 ± 9 ppm and a geometric albedo of $A_g = 0.23 \pm 0.05$. For KOI-196.01 Coughlin & López-Morales 2012 measure an eclipse depth of 75.4 ± 40.1 ppm and report a maximum albedo of $0.33_{-0.15}^{+0.16}$ and brightness temperature of $2463_{-168}^{+130.0}$ K.

For KOI-196.01, we find an eclipse depth of 46.2 ± 8.7 ppm, slightly lower than,

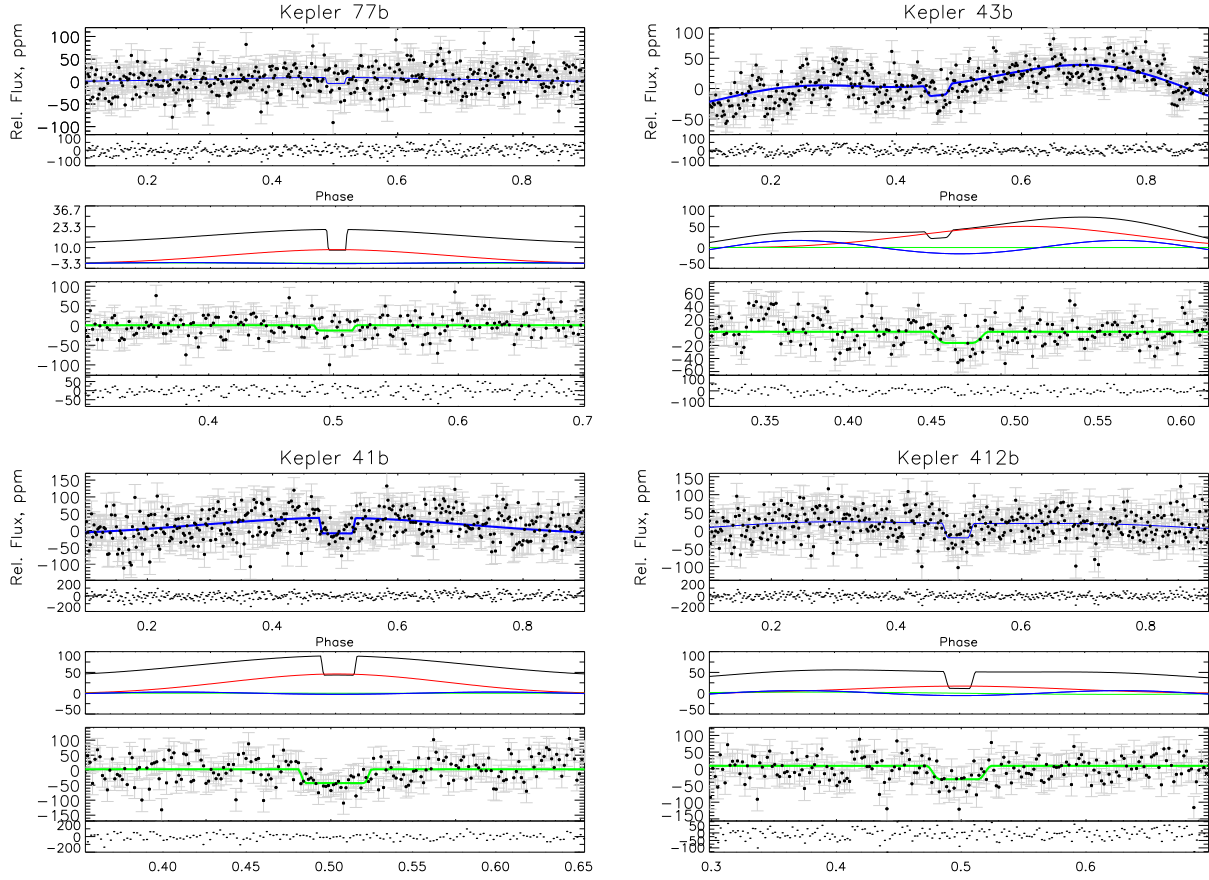


Fig. 3.— Fitted lightcurves for KOI-127.01/Kepler 77b (top, left), KOI-135.01/Kepler 43b (top, right), KOI-196.01/Kepler 41b (bottom, left) and KOI-202.01/Kepler 412b (bottom, right). In each quarter: Phase curve, residuals (top). Center: phasecurve contributions: Doppler (blue), ellipsoidal (green), planetary phase (red). Bottom: zoom into phase curve subtracted secondary eclipse, residuals.

but however consistent with Quintana et al. (2013) and Santerne et al. (2011a). Our fits correspond to a brightness temperature T_b of 2395^{+50}_{-58} K, a geometric albedo A_g of 0.18 ± 0.03 and a bond albedo A_b of 0.27 ± 0.05 . Figure 3 (bottom, left) shows our fit results for KOI-196.01.

3.1.12. KOI 202.01 / Kepler 412b

The planet Kepler 412b (Deleuil et al. 2014) is an inflated Jupiter with a mass of $0.94 \pm 0.09 M_{Jup}$ and a radius of $1.33 \pm 0.04 R_{Jup}$ orbiting its G3 V host star in 1.72 days . Deleuil et al. (2014) detected a secondary eclipse 47.4 ± 7.4 ppm and derived the day side temperature to be a maximum of 2380 ± 40 K and estimated the geometrical albedo, A_g , in the range 0.09 to 0.13 and a night side temperature of 2154 ± 83 K. For KOI-202.01 Coughlin & López-Morales 2012 measure an eclipse depth of 63.6 ± 37.7 ppm and report a maximum albedo of $0.19^{+0.1}_{-0.10}$ and brightness temperature of $2455^{+138.0}_{-207}$ K. Figure 3 (bottom, right) shows our fit results for Kepler 412b. Our analysis of Kepler 412b shows an eclipse depth of 40.2 ± 9.0 ppm, well within the lower end of the value of Deleuil et al. (2014). We therefore get a brightness temperature of 2355^{+35}_{-40} K, geometric albedo of 0.11 ± 0.02 , bond albedo of 0.16 ± 0.04 and a night side temperature of 2210^{+105}_{-163} K.

3.1.13. KOI 203.01 / Kepler 17b

Kepler 17b is a $M_P=2.45 \pm 0.11 M_{Jup}$ and $R_P=1.31 \pm 0.02 R_{Jup}$ planet orbiting a $1.02 \pm 0.03 R_{Sun}$ star with a period of 1.49 days (Endl et al. 2011). Endl et al. (2011) find measure an eclipse depth of 58 ± 10 ppm and a geometric albedo A_g of 0.1 ± 0.02 . Bonomo et al. (2012) find a slightly different $M_p = 2.47 \pm 0.10 M_{Jup}$ and $R_p = 1.33 \pm 0.04 R_{Jup}$ and an upper limit for the geometric albedo of $A_g < 0.12$. For KOI-203.01

Coughlin & López-Morales 2012 measure an eclipse depth of $52. \pm 98.0$ ppm and report a maximum albedo of $0.14_{-0.15}^{+0.14}$ and brightness temperature of $2319_{-4138}^{+202.0}$ K.

For KOI-203.01, we find an eclipse depth of 43.7 ± 6.4 ppm, a brightness temperature T_b of 2247_{-40}^{+35} K, a geometric albedo A_g of 0.08 ± 0.01 a bond albedo A_b of 0.13 ± 0.02 and an upper limit for the night side temperature T_{night} of 2229_{-58}^{+50} K. These results are slightly different from, but still consistent with Bonomo et al. (2012) and Endl et al. (2011). Figure 4 (top, left) shows our fit results for KOI 203.01.

3.1.14. KOI 204.01 / Kepler 44b

KOI-204.01 (Bonomo et al. 2012) is a $1.24 \pm 0.07 R_{Jup}$, $1.02 \pm 0.07 M_{Jup}$ planet orbiting its parent G2IV star in 3.25 days. For KOI-204.01 Coughlin & López-Morales 2012 measure an eclipse depth of 54.8 ± 82.5 ppm and report a maximum albedo of $1.92_{-1.74}^{+1.670}$ and brightness temperature of $2669_{-641}^{+231.0}$ K.

For KOI-204.01, we marginally detect a secondary eclipse with a depth of 21.9 ± 14.9 ppm. This corresponds to a brightness temperature T_b of 2348_{-279}^{+149} a geometric albedo A_g of 0.28 ± 0.19 , a bond albedo A_b of 0.42 ± 0.29 and an upper limit for the night side temperature T_{night} of 2347_{-280}^{+149} K. Figure 4 (top, right) shows our fit results for KOI 204.01.

3.1.15. KOI 428.01 / Kepler 40b

The planet KOI-428.01 ($1.17 \pm 0.04 R_{Jup}$; $2.2 \pm 0.4 M_{Jup}$), orbits an F5IV star of $2.13 \pm 0.06 R_{Sun}$, $1.48 \pm 0.06 M_{Sun}$, one of the largest and the most evolved stars discovered so far with a transiting planet (Santerne et al. 2011b).

For KOI-428.01, we detect an eclipse depth of 7.91 ± 7.55 ppm, consistent with a non

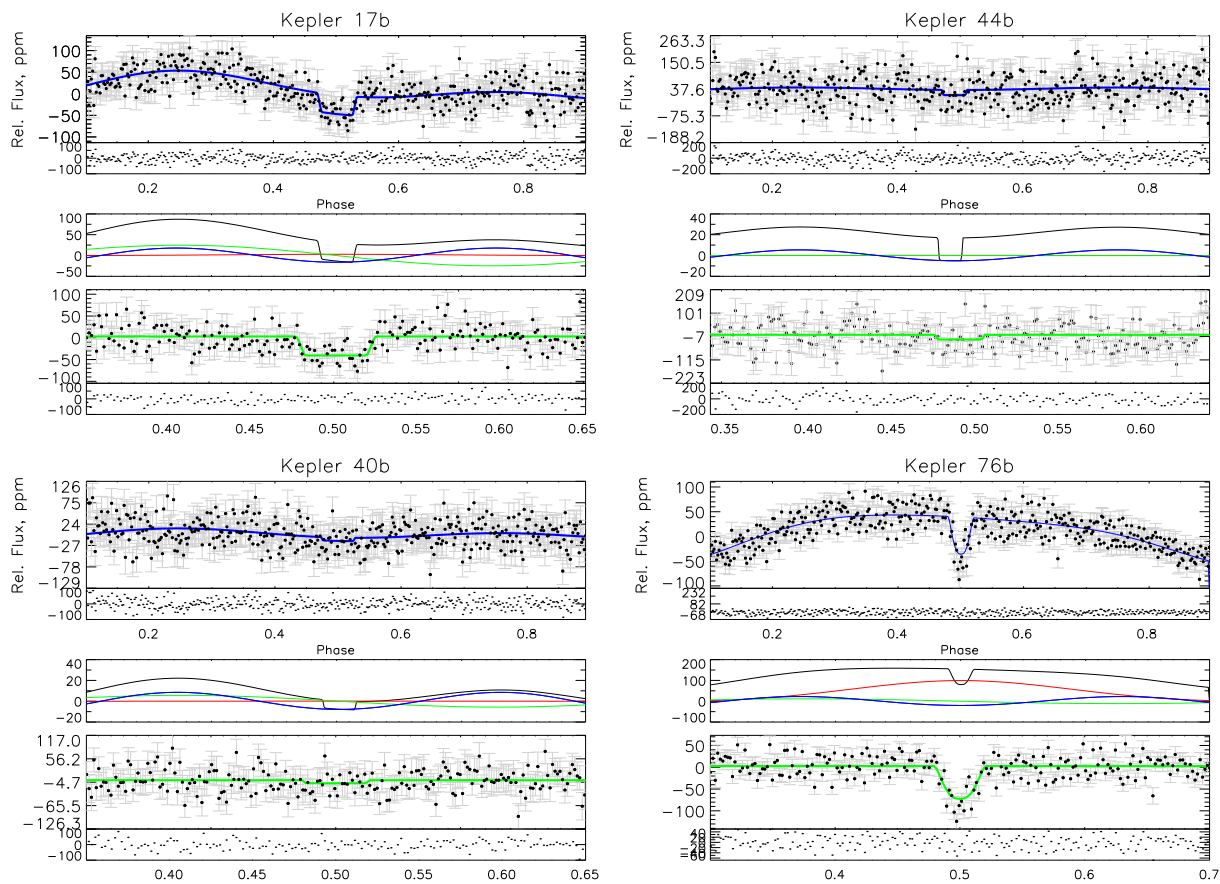


Fig. 4.— Fitted lightcurves for KOI-203.01/Kepler 17b (top, left) KOI-204.01/Kepler 44b (top, right), KOI-428.01/Kepler 40b (bottom, left) and KOI-1658.01/Kepler 76b (bottom, right). In each quarter: Phase curve, residuals (top). Center: phasecurve contributions: Doppler (blue), ellipsoidal (green), planetary phase (red). Bottom: zoom into phase curve subtracted secondary eclipse, residuals.

detection within one sigma. This corresponds to limits for the brightness temperature T_b of 2331_{-626}^{+193} K, the geometric albedo A_g of 0.09 ± 0.08 , the bond albedo A_b of 0.13 ± 0.13 and an upper limit for the night side temperature T_{night} of 2327_{-669}^{+195} K. Figure 4 (bottom, left) shows our fit results for KOI 428.01.

3.1.16. KOI 1658.01 / Kepler 76b

Kepler 76b (Faigler et al. 2013) ($2.0 \pm 0.26 M_{Jup}$, $1.25 \pm 0.08 R_{Jup}$) orbits a $1.2 M_{Sun}$ star in 1.55 days. It is slightly denser than Jupiter indicating that it is not inflated like other planets in this sample. Faigler et al. (2013) find a secondary eclipse depth of 98.9 ± 7.1 ppm as well as significant contribution to doppler, ellipsoidal and phase modulations of 13.5, 21.1 and 50.4 ppm.

For Kepler 76b, our model fits an eclipse of 75.6 ± 5.6 ppm, about 25% less than in Faigler et al. (2013). Using our values we find a brightness temperature of 2776_{-28}^{+26} K, a geometric albedo of 0.22 ± 0.02 and bond albedo of 0.33 ± 0.02 . Figure 4 (bottom, right) shows our fit results for KOI 1658.01. We find a Doppler boosting of 11.4 ± 1.0 and an ellipsoidal variation of 22.6 ± 1.9 , well in agreement with (Faigler et al. 2013). However, our derived phasecurve amplitude of 101.3 ± 3.6 is a factor two bigger than theirs. Reasons for this discrepancy – also in the derived eclipse depth – could be third light contributions ($f_3 = 0.056$, average third light fraction used in Faigler et al. 2013) or different stellar parameters (we used their TODMOR derived values from table 2 in Faigler et al. 2013, whereas they fitted to the values in table 1).

Table 3. Fit results for the amplitudes of phasecurve (A_p), Doppler boosting (A_d) and ellipsoidal variation (A_e), and eclipse depth D_{ecl} - all in ppm

KOI	A_p	A_d	A_e	D_{ecl}
1	3.0 ± 0.8	2.0 ± 0.2	2.9 ± 0.5	10.9 ± 2.2
2	60.8 ± 0.5	5.3 ± 0.1	16.8 ± 0.3	69.3 ± 0.5
10	13.8 ± 3.7	$< 1^a$	3.7 ± 2.0	16.5 ± 4.4
13	78.7 ± 5.4	$< 1^a$	37.1 ± 5.4	84.8 ± 5.4
17	9.5 ± 2.7	1.0 ± 0.9	$< 1^a$	11.3 ± 4.2
18	8.3 ± 2.6	$< 1^a$	3.1 ± 1.4	19.8 ± 3.6
20	16.7 ± 2.6	$< 1^a$	$< 1^a$	18.7 ± 4.9
97	47.8 ± 5.2	3.9 ± 4.0	$< 1^a$	46.6 ± 3.9
127	8.6 ± 5.4	$< 1^a$	$< 1^a$	13.3 ± 7.4
135	51.7 ± 3.3	$< 1^a$	16.9 ± 2.2	17.0 ± 5.3
196	46.3 ± 7.9	$< 1^a$	2.8 ± 4.3	46.2 ± 8.7
202	17.3 ± 7.4	2.7 ± 2.2	6.3 ± 3.9	40.2 ± 9.0
203	2.9 ± 5.9	24.7 ± 1.8	17.9 ± 3.2	43.7 ± 6.4
204	$< 1^a$	$< 1^a$	5.4 ± 4.8	21.9 ± 14.9
428	$< 1^a$	5.6 ± 2.1	8.5 ± 2.9	7.9 ± 7.5
1648	101.3 ± 3.6	11.4 ± 1.0	22.6 ± 1.9	75.6 ± 5.6

^aEquivalent to not detectable in our fit. In these cases the fitted values of the phase contributions converged in the (non-zero) minimum value of 10^{-7} - in other words these contributions were not needed to fit the data. Therefore we put in a conservative limit of $< 1ppm$.

Table 4. Derived brightness temperatures (T_b), geometric and bond albedos (A_g, A_b), equilibrium temperatures T_{eq} for no $f_{dist} = \frac{1}{2}$ and full redistribution $f_{dist} = \frac{2}{3}$ and night side temperature T_{night} .

KOI	T_b	A_g^a	A_b	$T_{1/2}^{eq}$	$T_{2/3}^{eq}$	T_{night}^b [K]
1	1947_{-45}^{+37}	0.05 ± 0.01	0.08 ± 0.02	1363	1574	1885_{-66}^{+51}
2	2897_{-3}^{+3}	0.27 ± 0.003	0.4 ± 0.003	1892	21858	2235_{-24}^{+3}
10	2241_{-76}^{+61}	0.11 ± 0.03	0.16 ± 0.04	1536	1774	1859^{+227}
13	3421_{-35}^{+32}	0.27 ± 0.02	0.40 ± 0.03	2620	3025	2394^{+251}
17	2060_{-96}^{+70}	0.07 ± 0.03	0.11 ± 0.04	1413	1632	1719^{+236}
18	2305_{-53}^{+45}	0.16 ± 0.03	0.25 ± 0.05	1429	1650	2169_{-113}^{+81}
20	2120_{-67}^{+54}	0.09 ± 0.02	0.14 ± 0.04	1422	1642	1711^{+223}
97	2547_{-28}^{+26}	0.32 ± 0.03	0.48 ± 0.04	1364	1575	–
127	2062_{-165}^{+100}	0.15 ± 0.09	0.23 ± 0.13	1136	1312	1854^{+216}
135	2295_{-95}^{+74}	0.06 ± 0.02	0.09 ± 0.03	1930	2229	–
196	2395_{-57}^{+50}	0.18 ± 0.03	0.27 ± 0.05	1513	1933	–
202	2355_{-40}^{+35}	0.11 ± 0.02	0.16 ± 0.04	1701	1965	2210_{-163}^{+105}
203	2247_{-40}^{+35}	0.08 ± 0.01	0.13 ± 0.02	1660	1917	2229_{-58}^{+50}
204	2348_{-277}^{+149}	0.28 ± 0.19	0.42 ± 0.29	1217	1405	2347_{-280}^{+149}
428	2331_{-627}^{+193}	0.09 ± 0.08	0.13 ± 0.13	1774	2048	2327_{-669}^{+195}
1658	2776_{-28}^{+26}	0.22 ± 0.02	0.33 ± 0.02	1875	2165	–

^aAlbedos corrected for thermal emission can be found in Table 5.

^bWhen the derived error bounds for some of the candidates included zero we did not give a lower limit for the night side temperature.

Table 5. Albedos corrected for thermal emission for no $f_{dist} = \frac{1}{2}$ and full redistribution

$$f_{dist} = \frac{2}{3}$$

KOI	A_g	$A_{g,c}(f_{dist} = \frac{1}{2})$	$A_{g,c}(f_{dist} = \frac{2}{3})$
1	0.05	0.03	-0.05 ^a
2	0.27	0.23	0.1
10	0.11	0.07	-0.06 ^a
13	0.27	0.09	-0.27 ^a
17	0.07	0.06	-0.03 ^a
18	0.16	0.15	0.08
20	0.09	0.07	-0.03 ^a
97	0.32	0.31	0.28
127	0.15	0.15	0.13
135	0.06	-0.01 ^a	-0.22 ^a
196	0.18	0.16	0.09
202	0.11	0.08	-0.05 ^a
203	0.08	0.05	-0.08 ^a
204	0.28	0.28	0.26
428	0.09	0.02	-0.21 ^a
1658	0.22	0.18	0.06

^aequivalent to a zero albedo

3.2. Non detections

For the following planets from our sample we were not able to detect secondary eclipses. The upper limits for secondary eclipse depths, albedos, and brightness temperatures of these candidates were calculated by adding the 1 sigma errors from the co-variance matrix to the best fit values.

3.2.1. *KOI 3.01 / HAT-P-11b / Kepler 3b*

HAT-P-11b (KOI 3.01 or Kepler 3b, Bakos et al. 2010) is a Hot Neptune type planet ($17M_e, 3.8R_e$) orbiting a bright ($V = 9.59$) and metal rich K4 dwarf star with a period of 4.89 days. This planet, that was already detected before the start of the *Kepler* mission is the brightest in our sample and the whole *Kepler* catalog with a magnitude of 9.174 in the *Kepler* band. Several other groups already analyzed the phasecurves with no detection of a secondary eclipse (e.g Southworth 2011, Deming et al. 2011 and Sanchis-Ojeda & Winn 2011). Figure 5 (top, left) shows our fit results for KOI 3.01.

The noise in KOI-3.01 is much bigger than in all other planets of our sample, which misleads our models to an unrealistic albedo value. However, given the orbital parameters, the maximum secondary eclipse depth we should ever find (assuming it is not self luminous) is 12 ppm. Therefore we did not carry through the temperature calculations for KOI-3.01.

3.2.2. *KOI 7.01 / Kepler 4b*

Kepler 4b (or KOI 7.01, Borucki et al. 2010a) is a $24.5 \pm 3.8M_e$ and $3.99 \pm 0.21R_e$ planet with period of 3.21 days around a 4.5 Gyr old near-turnoff G0 star. With a density of about $1.9 g/cm^3$ Kepler 4b is slightly denser and more massive than Neptune, but about

the same size. Kipping & Bakos (2011) exclude a secondary eclipse with an upper limit of 104 ppm for its depth, which corresponds to an upper limit for the brightness temperature of 3988K.

Our analysis confirms this and is also consistent with a non-detection to a level of < 9 ppm, which enables us to constrain the brightness temperature T_b to < 2797 K. Figure 5 (top, right) and Table 6 show our fit results for KOI 7.01.

3.2.3. KOI 98.01 / Kepler 14b

Kepler 14b (or KOI 98.01) is a $8.40 M_{Jup}$ and $1.136 R_{Jup}$ planet on a 6.79 day orbit around an F star in a binary system (Buchhave et al. 2011).

Our analysis, which used an additional polynomial fit to correct for systematics caused by a close visual binary, is the first of this kind for KOI-98.01. The results show an eclipse depth consistent with a non detection of < 10 ppm. This leads to a brightness temperature limit $T_b < 2415$ K, a geometric albedo $A_g < 0.17$. Figure 5 (bottom, left) and Table 6 show our fit results for KOI 98.01.

3.2.4. KOI 128.01 / Kepler 15b

Kepler 15b (Endl et al. 2011) is a $0.66 \pm 0.1 M_{Jup}$, $0.96 \pm 0.06 R_{Jup}$ planet in 4.94 day orbit around a metal-rich ($[Fe/H]=0.36 \pm 0.07$) G star; its mean density of $0.9 \pm 0.2 g/cm^3$ suggests a significant enrichment in heavy elements. Endl et al. (2011) find no sign of a secondary eclipse.

For KOI-128.01, we find an eclipse depth consistent with a non-detection of < 11 ppm. This corresponds to a brightness temperature T_b limit of < 2039 K and a geometric albedo

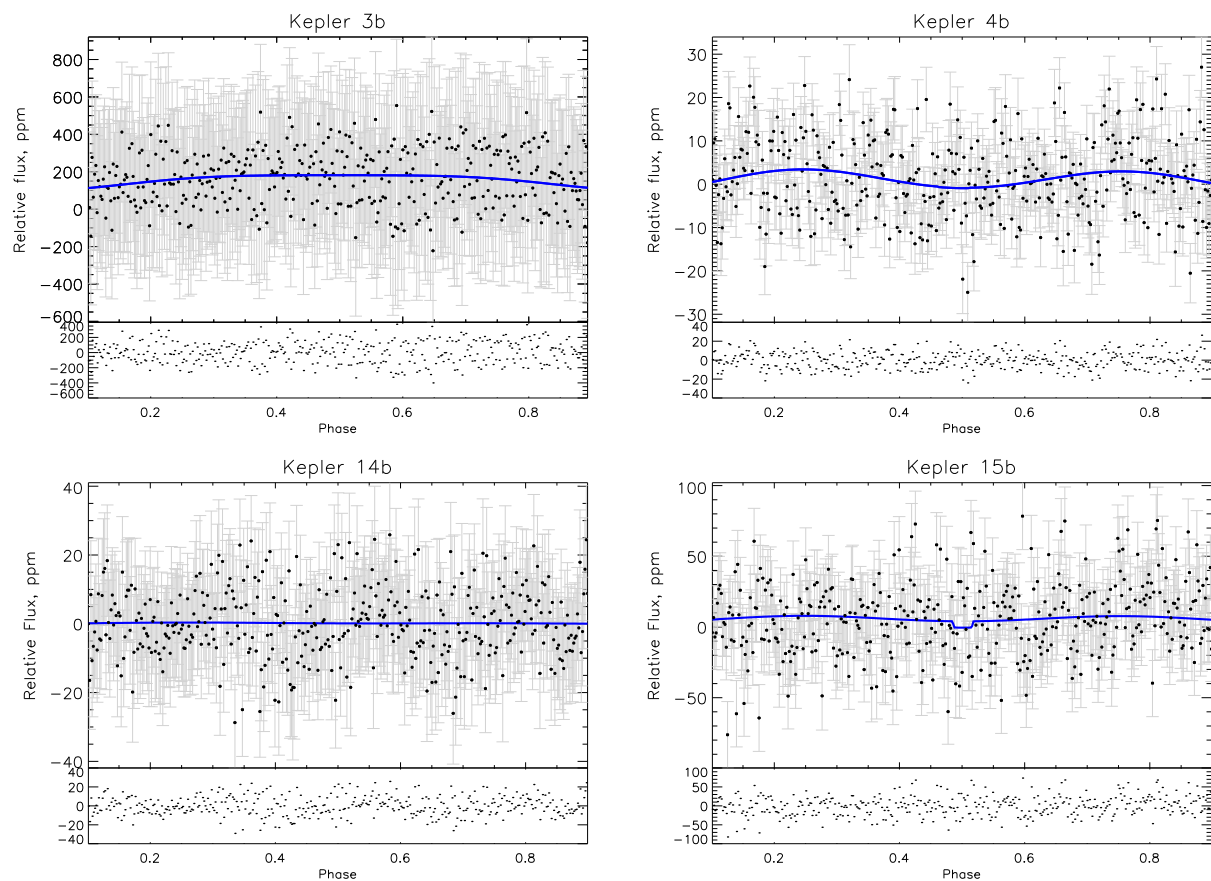


Fig. 5.— Fitted lightcurves for KOI-3.01/HAT-P-11b/Kepler 3b (top, left) KOI-7.01/Kepler 4b (top, right), KOI-98.01/Kepler 14b (bottom, left) and KOI-128.01/Kepler 15b (bottom, right). Blue curves are the best-fit model. None of these systems showed a significant secondary eclipse larger than our noise threshold. However, we were able to calculate upper limits for some of the parameters of these systems (see Table 6).

limit A_g of < 0.11 . Figure 5 (bottom, right) and Table 6 show our fit results for KOI 128.01. For KOI-128.01, we used the sum of the (0.5 sigma) detected secondary eclipse value and the error in that value as maximum detectable eclipse value.

3.3. Excluded planets

We also excluded planets from our sample that are part of multiple systems (e.g. Rowe et al. 2014), circumbinary planets (e.g. Doyle et al. 2011) and highly variable host star systems. Excluded multiple systems containing planets that fall into our sample are KOI 46 / Kepler 10, KOI 137 / Kepler 18, KOI 338 / Kepler 141, KOI 1779 / Kepler 318 and KOI 1805 / Kepler 319. We excluded KOI 63.01 / Kepler 63b (Sanchis-Ojeda et al. 2013) from our sample because we were not able to apply our methods. In this case the lightcurve was dominated by contributions from an additional signal with a different periodicity most probably induced by stellar activity.

3.4. The case of KOI 200 / Kepler 74b and KOI-2133 / Kepler 91b

The planet Kepler 74b (Hébrard et al. 2013) has mass and radius of $0.68 \pm 0.09 M_{Jup}$ and $1.32 \pm 0.14 R_{Jup}$ and orbits its F8V host star in 7.34 days. Kepler 91b (Lillo-Box et al. 2014) ($M_p = 0.88^{+0.17}_{-0.33} M_{Jup}$, $R_p = 1.384^{+0.011}_{-0.054} R_{Jup}$) orbits its host star ($R_* = 6.30 \pm 0.16 R_{Sun}$, $M_* = 1.31 \pm 0.10 M_{Sun}$) only $1.32^{+0.07}_{-0.22} R_*$ away from the stellar atmosphere at the pericenter. Lillo-Box et al. (2014) argue that Kepler 91b could therefore be at a stage of the planet engulfment and estimate that Kepler 91b will be swallowed by its host star in less than 55 Myr. They derive phasecurve parameters $A_e = 121 \pm 33$ ppm, $A_p = 25 \pm 15$ ppm and $A_d = 3 \pm 1$ ppm and no clear secondary eclipse, but 3 other dips in the lightcurve.

Table 6. Upper limits for planets without detected secondary eclipse.

KOI	ecl. depth [ppm]	T_b [K]	A_g	A_b
3 ¹	< 147	–	–	–
7	< 9	< 2797	< 0.62	< 0.93
98	< 10	< 2415	< 0.17	< 0.26
128 ²	< 11	< 2039	< 0.11	< 0.17

¹The noise in KOI-3.01 is much bigger than in all other planets of our sample, which misleads our models to an unrealistic albedo value. However, given the orbital parameters, the maximum secondary eclipse depth we should ever find (assuming it is not self luminous) is 12 ppm. Therefore we did not carry through the temperature calculations for KOI-3.01

²For KOI-128.01, we used the sum of the (0.5 sigma) detected secondary eclipse value and the error in that value as maximum detectable eclipse value.

Our analysis method (see blue fits in Figure 6) was not able to recover the signals from these lightcurves accurately. The reason is that both planets do not show a typical secondary eclipse signature, but instead also a series of extra dimmings at times other than of the expected eclipse (see grey Figure 6). The timing of some of these extra dips in the lightcurve at 0.166 of the period after transit and/or eclipse may be evidence for the presence of Trojan satellites - however, as also stated in Lillo-Box et al. (2014), this claim needs detailed stability studies to be confirmed. Another explanation is correlated noise and/or stellar activity dominating these lightcurves. We were not able to recover any useful results for the secondary eclipse depths and most of the other phase curve parameters and therefore were not able to compare to previous results and excluded these two targets from our analysis.

4. Summary and discussion

With our consistent analysis we were able to confirm and in most cases improve parameters derived by previous studies. We present new results for Kepler 1b-8b, 12b-15b, 17b, 40b, 41b, 43b, 44b, 76b, 77b, and 412b.

4.1. Comparison to other fitting routines - future improvements

For the cases of previously analyzed targets we were able to confirm (within less than 2σ for almost all cases) results derived from various previous or parallel analyses that used very different modeling approaches, from relatively simple boxcar fits (without a phase curve model) of only the secondary eclipse to very sophisticated Bayesian codes fitting all system parameters in an integrated way. The fact that we reproduce most of these results demonstrates the value of our compromise approach to combine a state-of-the-art

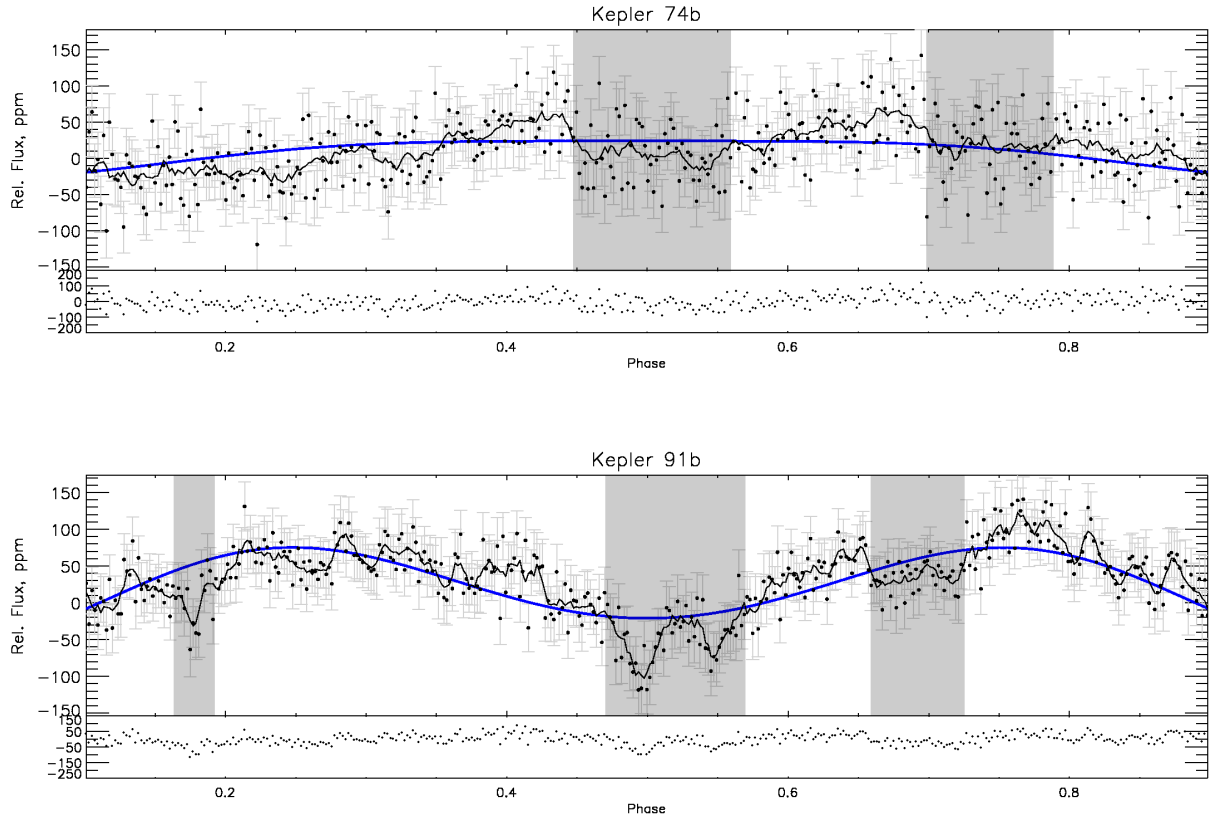


Fig. 6.— Lightcurves of the systems KOI-200/Kepler 74b (top) and KOI-2133/Kepler 91b (bottom). The grey regions of the lightcurves show extra dimmings that are not explainable with just a secondary eclipse. Our analysis method (blue fits) was not able to recover the secondary eclipse signals from these 'noisy' lightcurves accurately.

phasecurve model including all important contributions with a robust least-squares fit to trade off between number of systems and computing time. Also our goal was to focus on eclipses and phasecurves while fixing all other parameters to previously derived values. This significantly reduces the number of potential degeneracies that usually call for these more elaborated methods.

However, in order to increase the statistical relevance of our results we are currently working to extend the analysis to the whole sample of 489 Kepler Objects of Interest with $R_p > 4R_e$, $P < 10d$, $V_{mag} < 15$: we plan to apply EXONEST (Placek et al. 2014), a Bayesian model selection algorithm to the whole set of 489 candidates. With a sample of that size we hope to find statistically significant correlations of stellar and planetary parameters with the position of the planet, e.g., in albedo *vs* incoming flux phase space (see Figure 7).

4.2. Correlations with system parameters

For the following analysis of a potential correlation of the albedo with stellar or planetary parameters (see e.g. Figure 7) we used the albedo values, that were corrected for thermal emission (assuming no redistribution; $f_{dist} = 1/2$) that are shown in Table 5 (center).

Our results confirm the general trend of relatively low albedos for most of the Hot Jupiters, but we also show outliers with higher albedos.

We see no significant correlations in our data. Neither the stellar parameters ($[Fe/H]$ and $\log(g)$, see Figure 7) nor the planetary characteristics (mass, radius, density and surface gravity) correlate with the derived parameters. When excluding the planets with large errors in the albedo, there are indications that massive planets, very dense and very bloated

planets tend to be low in albedo – i.e., density extremes produce low albedos.

Even though we present a relatively large sample characterized in this comprehensive and consistent manner, our sample size is still too small to draw significant statistical conclusions. Future efforts will include analyzing all of the candidates as well as the complete Kepler dataset of 18 available quarters (Q0-Q17).

With *TESS* (Ricker et al. 2010) and *PLATO* (Rauer & Catala 2013; Hippke & Angerhausen 2015) on the horizon the future will bear an even bigger data set, marking great potential for characterizations in a similar way. Such future observations and analyses will include many more planets in a similar range of planetary and stellar parameters. A comparative analysis beyond their basic parameters of a large number of planets orbiting a variety of host stars will probe and eventually solve the fundamental underlying questions on planet formation, migration and composition.

We want to thank Martin Still (Director of the Kepler Guest Observer Office) for his valuable comments and frequent support on the use of PyKE. We thank Avi Shporer, Kevin Heng and the anonymous referee for valuable comments on the manuscript.

This research was supported by internal funds at the Rensselaer Polytechnic Institute. DA’s research was also supported by an appointment to the NASA Postdoctoral Program at the Goddard Space Flight Center, administered by Oak Ridge Associated Universities through a contract with NASA.

Facilities: Kepler.

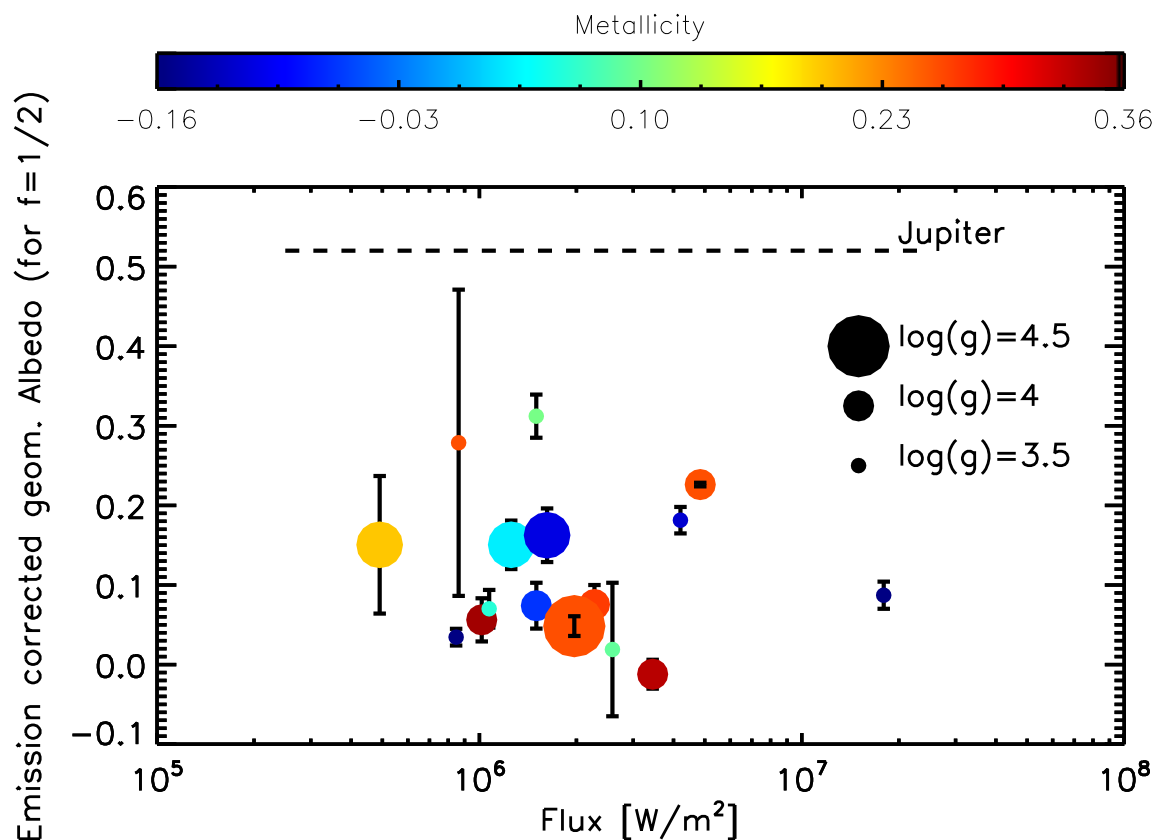


Fig. 7.— Emission-corrected geometric albedo $A_{g,c}$ for ($f = 1/2$) versus the incident stellar flux for our sample of Kepler giant planets (compare to Fig. 1 in Heng & Demory 2013). The colors represent the host star’s metallicity $[\text{Fe}/\text{H}]$ (see colorbar) and the size of the symbol corresponds to the host’s surface gravity $\log(g)$ (see legend). There is no obvious correlation with the distribution. The dashed line represents Jupiters’s albedo of 0.52 for comparison; all of the Hot Jupiters in our study have lower albedos.

REFERENCES

- Bakos, G. Á., Torres, G., Pál, A., et al. 2010, *ApJ*, 710, 1724
- Ballard, S., Fabrycky, D., Fressin, F., et al. 2011, *ApJ*, 743, 200
- Barclay, T., Huber, D., Rowe, J. F., et al. 2012, *ApJ*, 761, 53
- Barclay, T., Burke, C. J., Howell, S. B., et al. 2013, *ApJ*, 768, 101
- Batalha, N. M., Borucki, W. J., Bryson, S. T., et al. 2011, *ApJ*, 729, 27
- Batalha, N. M., Rowe, J. F., Bryson, S. T., et al. 2013, *ApJS*, 204, 24
- Bonomo, A. S., Hébrard, G., Santerne, A., et al. 2012, *A&A*, 538, A96
- Borucki, W. J., Koch, D., Jenkins, J., et al. 2009, *Science*, 325, 709
- Borucki, W. J., Koch, D. G., Brown, T. M., et al. 2010a, *ApJ*, 713, L126
- Borucki, W. J., Koch, D., Basri, G., et al. 2010b, *Science*, 327, 977
- Borucki, W. J., Koch, D. G., Basri, G., et al. 2011, *ApJ*, 736, 19
- Borucki, W. J., Agol, E., Fressin, F., et al. 2013, *Science*, 340, 587
- Buchhave, L. A., Latham, D. W., Carter, J. A., et al. 2011, *ApJS*, 197, 3
- Burke, C. J., Bryson, S. T., Mullally, F., et al. 2014, *ApJS*, 210, 19
- Burke, C. J., Christiansen, J. L., Mullally, F., et al. 2015, [arXiv:1506.04175](https://arxiv.org/abs/1506.04175)
- Claret, A., & Bloemen, S. 2011, *A&A*, 529, A75
- Coughlin, J. L., & López-Morales, M. 2012, *AJ*, 143, 39
- Cowan, N. B., & Agol, E. 2011, *ApJ*, 729, 54

- Deleuil, M., Almenara, J.-M., Santerne, A., et al. 2014, ArXiv e-prints, arXiv:1401.6811
- Deming, D., Sada, P. V., Jackson, B., et al. 2011, *ApJ*, 740, 33
- Demory, B.-O., & Seager, S. 2011, in *IAU Symposium*, Vol. 276, *IAU Symposium*, ed. A. Sozzetti, M. G. Lattanzi, & A. P. Boss, 475–476
- Demory, B.-O., Seager, S., Madhusudhan, N., et al. 2011, *ApJ*, 735, L12
- Demory, B.-O., de Wit, J., Lewis, N., et al. 2013, *ApJ*, 776, L25
- Désert, J.-M., Charbonneau, D., Fortney, J. J., et al. 2011, *ApJS*, 197, 11
- Doyle, L. R., Carter, J. A., Fabrycky, D. C., et al. 2011, *Science*, 333, 1602
- Dressing, C. D., & Charbonneau, D. 2013, *ApJ*, 767, 95
- Dunham, E. W., Borucki, W. J., Koch, D. G., et al. 2010, *ApJ*, 713, L136
- Endl, M., MacQueen, P. J., Cochran, W. D., et al. 2011, *ApJS*, 197, 13
- Esteves, L. J., De Mooij, E. J. W., & Jayawardhana, R. 2013, *ApJ*, 772, 51
- Faigler, S., & Mazeh, T. 2011, *MNRAS*, 415, 3921
- Faigler, S., Tal-Or, L., Mazeh, T., Latham, D. W., & Buchhave, L. A. 2013, *ApJ*, 771, 26
- Fortney, J. J., Demory, B.-O., Désert, J.-M., et al. 2011, *ApJS*, 197, 9
- Fressin, F., Torres, G., Charbonneau, D., et al. 2013, *ApJ*, 766, 81
- Gandolfi, D., Parviainen, H., Fridlund, M., et al. 2013, *A&A*, 557, A74
- Groot, P. J. 2012, *ApJ*, 745, 55
- Hébrard, G., Almenara, J.-M., Santerne, A., et al. 2013, *A&A*, 554, A114

- Heng, K., & Demory, B.-O. 2013, *ApJ*, 777, 100
- Henry, G. W., Marcy, G. W., Butler, R. P., & Vogt, S. S. 2000, *ApJ*, 529, L41
- Hippke, M., & Angerhausen, D. 2015, arXiv:1508.00427
- Hippke, M., & Angerhausen, D. 2015, arXiv:1503.03251
- Holman, M. J., Fabrycky, D. C., Ragozzine, D., et al. 2010, *Science*, 330, 51
- Howard, A. W., Marcy, G. W., Bryson, S. T., et al. 2012, *ApJS*, 201, 15
- Jenkins, J. M., Borucki, W. J., Koch, D. G., et al. 2010, *ApJ*, 724, 1108
- Jenkins, J. M., Twicken, J. D., Batalha, N. M., et al. 2015, *AJ*, 150, 56
- Kepler Mission Team. 2009, *VizieR Online Data Catalog*, 5133, 0
- Kipping, D., & Bakos, G. 2011, *ApJ*, 730, 50
- Kipping, D. M., Hartman, J., Buchhave, L. A., et al. 2013, *ApJ*, 770, 101
- Kipping, D. M., & Spiegel, D. S. 2011, *MNRAS*, 417, L88
- Kipping, D. M. 2010, *MNRAS*, 408, 1758
- Koch, D. G., Borucki, W. J., Rowe, J. F., et al. 2010, *ApJ*, 713, L131
- Latham, D. W., Borucki, W. J., Koch, D. G., et al. 2010, *ApJ*, 713, L140
- Lillo-Box, J., Barrado, D., Moya, A., et al. 2014, *A&A*, 562, A109
- Line, M. R., Liang, M. C., & Yung, Y. L. 2010, *ApJ*, 717, 496
- Masuda, K. 2015, *ApJ*, 805, 28
- Mazeh, T., Nachmani, G., Sokol, G., Faigler, S., & Zucker, S. 2012, *A&A*, 541, A56

- Mislis, D., & Hodgkin, S. 2012, MNRAS, 422, 1512
- Morris, B. M., Mandell, A. M., & Deming, D. 2013, ApJ, 764, L22
- Moses, J. I., Visscher, C., Fortney, J. J., et al. 2011, ApJ, 737, 15
- Mullally, F., Coughlin, J. L., Thompson, S. E., et al. 2015, ApJS, 217, 31
- O’Donovan, F. T., Charbonneau, D., Mandushev, G., et al. 2006, ApJ, 651, L61
- Pál, A., Bakos, G. Á., Torres, G., et al. 2008, ApJ, 680, 1450
- Petigura, E. A., Howard, A. W., & Marcy, G. W. 2013, Proceedings of the National Academy of Science, 110, 19273
- Placek, B., Knuth, K. H., & Angerhausen, D. 2014, ApJ, 795, 112
- Quintana, E. V., Rowe, J. F., Barclay, T., et al. 2013, ApJ, 767, 137
- Quintana, E. V., Barclay, T., Raymond, S. N., et al. 2014, Science, 344, 277
- Rauer, H., & Catala, C. a. a. 2013, ArXiv e-prints, arXiv:1310.0696
- Ricker, G. R., Latham, D. W., Vanderspek, R. K., et al. 2010, in Bulletin of the American Astronomical Society, Vol. 42, American Astronomical Society Meeting Abstracts 215, 450.06
- Rogers, J., López-Morales, M., Apai, D., & Adams, E. 2013, ApJ, 767, 64
- Rowe, J. F., Bryson, S. T., Marcy, G. W., et al. 2014, ApJ, 784, 45
- Rowe, J. F., Coughlin, J. L., Antoci, V., et al. 2015, ApJS, 217, 16
- Russell, H. N. 1916, ApJ, 43, 173
- Sanchis-Ojeda, R., & Winn, J. N. 2011, ApJ, 743, 61

- Sanchis-Ojeda, R., Winn, J. N., Marcy, G. W., et al. 2013, *ApJ*, 775, 54
- Santerne, A., Bonomo, A. S., Hébrard, G., et al. 2011a, *A&A*, 536, A70
- Santerne, A., Díaz, R. F., Bouchy, F., et al. 2011b, *A&A*, 528, A63
- Santerne, A., Moutou, C., Barros, S. C. C., et al. 2012, *A&A*, 544, L12
- Shporer, A., Kaplan, D. L., Steinfadt, J. D. R., et al. 2010, *ApJ*, 725, L200
- Shporer, A., Jenkins, J. M., Rowe, J. F., et al. 2011, *AJ*, 142, 195
- Shporer, A., O’Rourke, J. G., Knutson, H. A., et al. 2014, *ApJ*, 788, 92
- Smith, J. C., Stumpe, M. C., Van Cleve, J. E., et al. 2012, *PASP*, 124, 1000
- Southworth, J. 2011, *MNRAS*, 417, 2166
- Still, M., & Barclay, T. 2012, *PyKE: Reduction and analysis of Kepler Simple Aperture Photometry data*, astrophysics Source Code Library, ascl:1208.004
- Stumpe, M. C., Smith, J. C., Van Cleve, J. E., et al. 2012, *PASP*, 124, 985
- Szabó, G. M., Pál, A., Derekas, A., et al. 2012, *MNRAS*, 421, L122
- Visscher, C., & Moses, J. I. 2011, *ApJ*, 738, 72